



Research article

Synergistic bactericidal combinations between gentamicin and chitosan capped ZnO nanoparticles: A promising strategy for repositioning this first-line antibiotic

Ivana R. Scolari, Paulina L. Páez, Gladys E. Granero*

Unidad de Investigaciones y Desarrollo en Tecnología Farmacéutica (UNITEFA)-CONICET, Departamento de Ciencias Farmacéuticas, Facultad de Ciencias Químicas, Universidad Nacional de Córdoba, Argentina

ARTICLE INFO

Keywords:

Gentamicin
Zinc oxide nanoparticles (ZnO NPs)
Synergic bactericidal activity
Reactive oxygen species (ROS)

ABSTRACT

Gentamicin (GEN), a widely used broad-spectrum antibiotic, faces challenges amid the global emergency of antimicrobial resistance. This study aimed to explore the synergistic effects of zinc oxide nanoparticles (ZnO NPs) in combination with GEN on the bactericidal activity against various bacterial strains. Results showed ZnO NPs with MICs ranging from 0.002 to 1.5 $\mu\text{g}/\text{mL}$, while the precursor salt displayed a MIC range of 48.75–1560 $\mu\text{g}/\text{mL}$. Chitosan (CS)-capped ZnO NPs exhibited even lower MICs than their uncapped counterparts, with the CS-capped synthesized ZnO NPs demonstrating the lowest values. Minimal bactericidal concentrations (MBC) aligned with MIC trends. Combinations of CS-capped synthesized ZnO NPs and GEN proved highly effective, inhibiting bacterial growth at significantly lower concentrations than GEN or ZnO NPs alone. This phenomenon may be attributed to the conformation of CS on the ZnO NPs' surface, enhancing the positive particle surface charge. This possibly facilitates a more effective interaction between ZnO NPs and microorganisms, leading to increased accumulation of zinc and GEN within bacterial cells and an overproduction of reactive oxygen species (ROS). It's crucial to note that, while this study did not specifically involve resistant strains, its primary focus remains on enhancing the overall antimicrobial activity of gentamicin. The research aims to contribute to addressing the global challenge of antimicrobial resistance, recognizing the urgent need for effective strategies to combat this critical issue. The findings, particularly the observed synergy between ZnO NPs and GEN, hold significant implications for repositioning the first-line antibiotic GEN.

1. Introduction

Gentamicin (GEN) is a broad-spectrum antibiotic that belongs to the family of aminoglycoside antibiotics that have proven to be clinically very effective to treat infections caused by Gram-negative bacteria such as *Escherichia coli*, *Klebsiella*, *Acinetobacter*, *Pseudomonas aeruginosa*, and some Gram-positive bacteria like *staphylococci* and *streptococci* [1]. However, the alarming rise of antibiotic-resistant strains substantially threatens global healthcare [2]. To address this challenge, strategies beyond traditional antibiotic use are essential. One effective approach involves synergistically combining antibiotics with other agents, thereby enhancing their spectrum of activity. For instance, GEN was combined with quercetin [1], a biofilm inhibitor. It was found that this

* Corresponding author.

E-mail address: glagranero@unc.edu.ar (G.E. Granero).

combination had a better anti-bacterial biofilm activity than GEN or quercetin alone. Jiang et al. [3], discovered that GEN plus fructose exhibited a synergy antibiotic effect on *Salmonella* infections in chickens. Zhou et al. [4], displayed that the exogenous supplementation of D-ribose was an adjuvant able to promote the effect of GEN on multidrug-resistant *Salmonella*.

Although GEN has been frequently used in a synergistic combination with other antibiotics in clinical practice against *S. aureus*, the Infectious Diseases Society of America (IDSA) guidelines do not recommend this therapeutic strategy because of potential nephrotoxicity problems [5]. In this context, several novel approaches are aimed at finding alternative strategies for increasing antibiotic efficacy, among them is the combination of commercial antibiotics with metal nanoparticles (MNPs) [6]. Within this category are zinc oxide nanoparticles (ZnO NPs), which have been shown to have widespread antibacterial properties [4,7–9]. Moreover, ZnO NPs are listed by the US Food and Drug Administration (FDA) as “Recognized as Safe (GRAS)”. Select committee on GRAS substances (SCOGS) opinion: tannic acid (hydrolyzable gallotannins) [10].

Besides their intrinsic antibacterial properties, ZnO NPs combined with rifampicin could reduce its minimum inhibitory concentration (MIC) against *Mycobacterium smegmatis* by 4 times [11]. Also, the combination of ampicillin with ZnO NPs increased the ampicillin antibacterial activity against *Citrobacter freundii* [12]. Furthermore, various studies have shown that the association of ZnO NPs with several antibiotics resulted in an increase in their inhibition halos against different bacteria [13]. Therefore, taking advantage of the antibacterial performance and the potential synergistic effects of ZnO NPs when combined with common antibiotics, in conjunction to retain GEN in the antibacterial arsenal.

Chitosan, a derivative of chitin, has garnered significant attention in various scientific studies [14–16]. Its widespread application is particularly notable in enhancing antibacterial activity when employed as a surface coating. The unique properties of chitosan, such as biocompatibility, biodegradability, and antimicrobial efficacy, make it an ideal candidate for coating surfaces. The positive charge of chitosan molecules facilitates interactions with negatively charged bacterial cell membranes, leading to membrane disruption and increased permeability. Additionally, chitosan’s ability to form a protective layer on surfaces provides a physical barrier against bacterial adhesion and biofilm formation. This versatile biopolymer, derived from natural sources, holds promise for various biomedical and industrial applications, contributing to the development of advanced materials with improved antibacterial properties [17–20].

The present study sought to investigate whether chitosan (CS)-coated ZnO NPs enhance the antibacterial activity of GEN. The aim was to highlight how these combinations can offer benefits, such as increased efficacy, reduced doses of individual drugs, and increased intracellular concentrations. These mechanisms underscore the potential of synergistic antimicrobial combinations to prevent or reduce the emergence of antibiotic resistance.

2. Experimental section

2.1. Materials

Zinc acetate dihydrate ($\text{Zn}(\text{CH}_3\text{COO})_2 \cdot 2\text{H}_2\text{O}$) was purchased from Pura Química (Córdoba, Argentina). Chitosan (CS; low molecular weight 50–190 kDa, 85 % degree of deacetylation) was purchased from Sigma Aldrich. Commercial ZnO NPs were purchased from Sigma Aldrich (nanopowder <100 nm particle size Lot#MKCB2717V). Gentamicin was purchased from Sigma Aldrich. The Müller-Hinton broth (MHB, Britania S.A.®, Buenos Aires, Argentina). Resazurin sodium salt was obtained from Sigma Aldrich. The reagents of analytical grade were used without further purification.

2.2. Synthesis and characterization of ZnO NPs and chitosan (CS)-capped ZnO NPs

2.2.1. Synthesis of zinc oxide nanoparticles (ZnO NPs)

ZnO NPs were synthesized by adding drop-wise to 5 % w/v zinc acetate dihydrate in Milli-Q water, a 1 M NaOH aqueous solution to adjust the pH to 14 under continuous stirring at 300 rpm and t 70 °C. This mixture was stirred continuously for 3 h at 70 °C. The resulting precipitate was collected from the suspension by 5 spin cycles at 3500 rpm, at 25 °C for 5 min, and washed with Milli-Q water. Finally, the resultant wet power was dried in an oven at 70 °C for 18 h to ensure the complete transformation of $\text{Zn}(\text{OH})_2$ to ZnO NPs.

2.2.2. Coating of ZnO NPs with chitosan (CS)

To obtain the CS-capped ZnO NPs, a 2.5 % w/v CS solution in 1 % v/v acetic acid was prepared whose pH was adjusted to 4.5 with a 1 M NaOH solution. To prepare the CS-capped ZnO NPs, 1 mg of marketed ZnO NPs or ZnO NPs synthesized following the method described in the previous section were added to a mixture of 2.5 mL of Milli-Q water and 2.5 mL of the 2.5 % w/v CS aqueous solution and stirred at 300 rpm at room temperature for 24 h, respectively. After that, the CS-capped ZnO NPs were separated from the mixture by centrifugation at 3500 rpm for 5 min. The white precipitate was rinsed with three washing cycles at 3500 rpm for 5 min with Milli-Q water and then, samples were dried in an oven at 70 °C for 24 h.

2.2.3. Characterization techniques

The particle size and surface charge were measured by dynamic light scattering (DLS) and ζ potential measurements, respectively, using a DLS (ZetasizerNano ZS, Malvern, UK). The diameter and PDI of particle size of NPs were estimated using the CONTIN algorithm analysis through inverse Laplace Transformation of the autocorrelation function. The morphologies and distribution of the ZnO NPs and CS-capped ZnO NPs were determined by using a FE-SEM Sigma analytical scanning electron microscope on a Carl Zeiss Sigma at an intensity of 5 kV. The size distributions of the nanoparticles were also evaluated by measuring the diameter of 100 nanoparticles from

the randomly selected SEM images using ImageJ software. The crystal phases of ZnO NPs were detected by X-ray diffraction (XRD, Philips-PW1800) in the range $2\theta = 5^\circ\text{--}80^\circ$. The total zinc content from ZnO NPs and CS-capped ZnO NPs was determined by atomic absorption spectrophotometry (AAS, Thermo Fisher iCE 3000) after dissolving the particles in HNO_3 . A lamp at a wavelength of 213.9 nm with a bandpass of 0.2 nm was used. Background correction was achieved with a deuterium lamp. The calibration curve was prepared with the zinc acetate salt in the range of 0.098 at $1.56\ \mu\text{g}/\text{mL}$. For thermogravimetric analysis (TGA), samples were placed in platinum pans and heated from 25 to $600\ ^\circ\text{C}$, at a heating rate of $10\ ^\circ\text{C}\ \text{min}^{-1}$, under a nitrogen flow of $50\ \text{mL}\ \text{min}^{-1}$ in a thermal analyzer TGA-DSC Instrument, Discovery series.

2.3. Microbiological assays

2.3.1. Bacterial strains

The gram-negative *Escherichia coli* ATCC 25922 and *Pseudomonas aeruginosa* ATCC 27853 and the gram-positive *Staphylococcus aureus* ATCC 29213 and *Enterococcus faecalis* ATCC 29212 strains from the American Type Culture Collection (ATCC) were evaluated.

2.3.2. Determination of minimum inhibitory concentration (MIC) and minimal bactericidal concentration (MBC)

The minimum inhibitory concentration (MIC) for each antimicrobial agent was determined by the microdilution broth technique with a 96-well microplate and using Müller–Hinton broth (MHB, Britania S.A.®, Buenos Aires, Argentina) as an antibacterial assay medium following the Clinical and Laboratory Standards Institute (CLSI) guidelines [21]. GEN and ZnO NPs, commercially available or synthesized, with or without capped with CS, respectively, were evaluated at two-fold serial dilution to obtain the following range of concentrations: 50 to $0.024\ \mu\text{g}/\text{mL}$ for GEN and 1 to $0.001\ \mu\text{g}/\text{mL}$ of zinc content from ZnO NPs and CS-capped ZnO NPs, respectively. After that, $100\ \mu\text{L}$ of a bacterial suspension ($5 \times 10^6\ \text{CFU}/\text{mL}$) was added to each well. The bacterial suspension without any treatment was added in triplicate as a growth control. The negative control contained only the MHB. Plates were incubated for 24 h at $37\ ^\circ\text{C}$. MIC was defined as the first dilution with no visible bacterial growth after 24 h of incubation at $37\ ^\circ\text{C}$ and was determined by triplicate. To confirm the MIC value obtained by visual observation of turbidity, $3\ \mu\text{L}$ of $1\ \text{mg}/\text{mL}$ resazurin sodium salt was added. Resazurin is a redox indicator of cellular metabolism, viable bacterial cells reduce non-fluorescent resazurin (blue) to fluorescent resorufin (pink). In this case, the MIC value was considered the lowest concentration where a color blue was observed.

The minimum bactericidal concentration (MBC) was performed following the MIC assay by inoculating $20\ \mu\text{L}$ of each well with no visible growth, before adding resazurin, for 24 h at $37\ ^\circ\text{C}$ and recording the number of bacterial colonies after incubation. MBC was defined as the lowest concentration of each antimicrobial agent that kills 99.9 % of bacteria.

2.3.3. Checkerboard testing and determination of the fractional inhibitory concentration index (FICI)

The synergistic, additive, indifferent, or antagonistic effects of the combination of GEN with the synthesized CS-capped ZnO NPs were determined with the microdilution method by serially diluting GEN in the x-axis and CS-capped ZnO NPs synthesized in the y-axis [22] $100\ \mu\text{L}$ of a bacterial suspension ($5 \times 10^6\ \text{CFU}/\text{mL}$) were added to each well of the 96-well plate and incubated at $37\ ^\circ\text{C}$ for 24 h. The FICI was calculated with the following Equation (1).

$$FICI = \frac{MIC\ A\ with\ B}{MIC\ A} + \frac{MIC\ B\ with\ A}{MIC\ B} \quad (1)$$

Synergy was defined as the FICI values ≤ 0.5 , additive $>0.5\ y \leq 1$, indifferent $>1\ y \leq 4$ and antagonism by FICI values > 4 .

2.3.4. Determination of reactive oxygen species (ROS) in bacterial cells

The intracellular bacterial reactive oxygen species (ROS) levels generated after treatment with CS-capped and uncapped ZnO NPs, GEN, or the combination CS-capped and uncapped ZnO NPs/GEN, respectively, were determined in *Staphylococcus aureus* ATCC 29213, *Escherichia coli* ATCC 25922, *Pseudomonas aeruginosa* ATCC 27853, and *Enterococcus faecalis* ATCC 29212 with the 2,7-dichlorodihydrofluorescein diacetate (DCFH-DA) assay [23]. The concentrations used corresponded to the concentrations of maximum synergistic activity of CS-capped and uncapped ZnO NPs, GEN alone or their combinations were incubated with the tested bacteria for 0 and 1 h at $37\ ^\circ\text{C}$. Then, $200\ \mu\text{L}$ of each sample were placed in 96-well plates in triplicate and treated with $20\ \mu\text{L}$ of 10 mM DCFH-DA reagent in the dark, a nonfluorescent compound, which could react with ROS to transform into a fluorophore. The DCFH-DA treated bacterial cells were incubated 30 min and then the fluorescence was determined by fluorescence spectroscopy in BioTek Synergy™ HT Microplate Reader, at an excitation and emission wavelength of 488 nm and 535 nm, respectively. In addition, the samples were observed by microscopy. The green fluorescence intensity of bacteria was recorded using a Leica DMI 8 microscope.

2.3.5. Oxidative stress determined by glutathione (GSH) effect

To evaluate the link between the level of oxidative stress produced through ROS generation by the synergistic combination between GEN and synthesized CS-capped ZnO NPs and their enhanced antibacterial activity mechanism, the glutathione (GSH) depletion ability by neutralizing ROS through its oxidation into glutathione disulfide (GSSG) was investigated [24]. Briefly, to a 0.1 mL of bacterial suspension ($\text{OD}_{600\ \text{nm}}\ 1.0$) was added GEN, CS-capped synthesized ZnO NPs, and the GEN/CS-capped synthesized ZnO NPs combination, respectively, and supplemented with $10\ \mu\text{L}$ of a 1 mM GSH solution in PBS. The mixture was incubated at $37\ ^\circ\text{C}$ for 1 h. Then, samples were treated with $10\ \mu\text{L}$ of 10 mM DCFH-DA reagent in the dark and incubated for 30 min. The ROS were determined by fluorescence spectroscopy determined by fluorescence spectroscopy (BioTek Synergy™ HT Microplate Reader) at an excitation and emission wavelength of 488 nm and 535 nm, respectively. The negative control was a bacterial suspension with GSH solution and

without any treatment.

2.4. Determination of intracellular zinc levels after bacterial internalization of ZnO NPs and CS-capped ZnO NPs

The MIC concentrations of ZnO NPs and CS-capped ZnO NPs, respectively, or zinc acetate dihydrate were added to the respective bacterial suspension (5×10^6 CFU/mL), and cells were incubated for 1 h at 37 °C. After that, the culture was centrifuged at 8000 rpm for 5 min. Then, the supernatant was removed and the cell pellets were resuspended with 0.5 mL of PBS and subjected to 3 cycles of freezing in an ultrafreezer at -39 °C and heating in an oven at 60 °C for 30 min each, interspersed with 10 min of sonication. They were subsequently digested with 10 % v/v concentrated HNO₃ and 0.5 mL was taken in a final volume of 10 mL of 10 % HNO₃. The digested samples of bacterial cells and ZnO NPs, with or without capped, zinc atoms were measured by AAS.

2.5. Determination of intracellular gentamicin levels after bacterial internalization combined with CS-coated synthesized ZnO NPs

2.5.1. Validation of an indirect UV–visible spectrophotometric method for gentamicin quantification

Gentamicin (GEN) exhibits poor absorption of ultraviolet and visible light, necessitating the use of an indirect spectrophotometric method for its quantification. The colorimetric reaction with ninhydrin (NIN) is commonly employed for the qualitative identification of various drugs containing amino groups. The validation of the indirect UV–visible spectrophotometric method adhered to the criteria outlined in the ICH and FDA guidelines, focusing on specificity/selectivity, linearity, accuracy, limit of detection (LOD), limit of quantification (LOQ), and precision (intra-day and inter-day) parameters [25,26].

To assess the specificity or selectivity of the method, UV–visible absorption spectra ranging from 200 to 800 nm were recorded. Various solutions were prepared, including 1 µg/mL CS-capped ZnO NPs (with and without NIN), 1.25 % w/v NIN, 25 µg/mL GEN, a solution of 25 µg/mL GEN with 1.25 % w/v NIN, and the supernatant of bacterial strains (without GEN) with and without NIN. All solutions were prepared in PBS, with PBS serving as the background correction. The calibration curve was generated using GEN sulfate solutions at seven different concentrations in PBS within the range of 100 to 3.125 µg/mL.

For the colorimetric reaction, 50 µL of a 1.25 % w/v NIN solution prepared in PBS was added to 5 mL of GEN (1:10 ratio). The samples were heated at 95 °C for 5 min in a thermostatic bath, subsequently cooled with an ice bath, and quantified using a UV–visible spectroscopy Agilent Technologies Cary 60 UV–Vis® spectrophotometer in the range of 200–800 nm [27,28]. The LOD of the method was determined by the analyte concentration exhibiting a peak area ratio three times greater than the baseline noise. The LOQ was defined as the analyte concentration yielding a peak area ratio ten times higher than the baseline noise.

To evaluate the precision parameters of the proposed analytical method, three GEN concentration values were chosen: low (L): 3.125 µg/mL, medium (M): 25 µg/mL, and high (H): 100 µg/mL. Three measurements were taken for each sample. Intra-day precision involved consecutive measurements on the same day, while inter-day precision encompassed measurements on two different days. The average and standard deviation (SD) values for GEN were calculated, and precision was expressed as the relative standard deviation (RSD) according to Equation (2).

$$RSD (\%) = \frac{SD}{Mean} \times 100 \quad (2)$$

The accuracy was assessed through the percentage recovery (Recovery %) of the analyte at three concentration levels (L, M, and H). The recovery % of GEN was calculated using Equation (3).

$$Recovery (\%) = \frac{Observed\ concentration}{Expected\ concentration} \times 100 \quad (3)$$

2.5.2. Intracellular determination assay of gentamicin

To 700 µL of a bacterial suspension (5×10^6 CFU/mL) in PBS was added 700 µL of a GEN solution in PBS or 700 µL the synergic combination GEN/CS-capped synthesized ZnO NPs in PBS. Then, mixtures were incubated at 37 °C for 1 h and centrifuged at 8000 rpm for 5 min. The supernatant was then removed and the cell pellets were resuspended in 1 mL of PBS and subjected to 3 cycles of freezing in a deep freezer at -39 °C and heating in an oven at 60 °C for 30 min each, interspersed with 10 min of sonication. Subsequently, 50 µL of acetone was added and centrifuged at 8000 rpm for 5 min to separate the CS and the acetone-insoluble proteins. After that, 1 mL of the supernatant was taken out to which 10 µL of 1.25 % w/v NIN previously prepared in PBS was added. Samples were heated at 95 °C for 5 min in a thermostatic bath, subsequently cooled with an ice bath, and quantified by UV–visible spectroscopy Agilent Technologies Cary 60 UV–Vis® spectrophotometer) at 400 nm. In this way, the amount of intracellular GEN was quantified.

2.6. Data analyses

Quantitative data are expressed as the mean \pm standard deviation (SD). One-way analysis of variance (ANOVA) was used to carry out the statistical analysis. A significance level value between groups of $p < 0.05$ was considered significant.

3. Results and discussion

3.1. Characterization of nanoparticles (NPs)

Table 1 shows average hydrodynamic particle size, polydispersity index (PDI), and zeta potential values (ζ -potential) obtained from DLS. The commercialized ZnO NPs were larger compared to the synthesized ZnO NPs. However, in both cases the PDI was less than 0.25, meaning that the size distribution of the ZnO NPs was homogeneous. Both ZnO NPs had a ζ -potential negative of approximately -22 mV. This high ζ -potential value indicated that ZnO NPs were moderately stable because of electrical repulsion between the NPs preventing their aggregation. Both commercial and synthesized ZnO NPs coating with CS slightly increased in size, although their PDI values remained less than 0.25, so the distribution of both CS-capped ZnO NPs was kept homogeneous. However, the ζ -potential values of these CS-capped ZnO NPs changed to positive values with values higher than 30 mV, evidencing the presence of CS, a positively charged polyelectrolyte, onto the surface of the ZnO NPs. Therefore, both types of CS-capped ZnO NPs were electrically stable.

The X-ray patterns of ZnO NPs, commercialized and synthesized, with or without coating with CS, zinc acetate dihydrate and CS are displayed in Fig. 1. The x-ray diffraction (XRD) patterns of both commercial (Fig. 1A) and synthesized ZnO NPs (Fig. 1B) showed the diffraction peaks located at 2θ values of 31.76° , 34.41° , 36.25° , 47.52° , 56.58° , 62.84° and 67.92° , which were consistent with the (100), (002), (101), (102), (110), (103), and (112) reflection planes of the hexagonal structure of ZnO described in JCPDS (JCPDS: 01-080-0074) (Joint Committee on Powder Diffraction Standards) [29]. Therefore, both commercial and synthesized ZnO NPs had a hexagonal structure with sharp diffraction peaks, indicating good crystallinity [30]. On the other hand, no traces of the zinc acetate dihydrate (Fig. 1F), the precursor salt in the synthesis of ZnO NPs, were evident in the XRD pattern of synthesized ZnO NPs (Fig. 1B), indicating that the ZnO NPs were pure without the presence of contamination from its precursor. On the other hand, XRD patterns of both, commercially available and synthesized, CS-capped ZnO NPs (Fig. 1C and D) displayed that their peak intensities were reduced. The ratio of intensities between the 100/002 peaks of uncapped and capped ZnO NPs was modified, from 0.9 to 0.8, respectively, and the intensities ratio between the 101/002 peaks, changed from 1.6 to 1.3, respectively. Also, a slight broadening of all peaks was observed in the XRD patterns from the CS-capped ZnO NPs in comparison with the XRD patterns from the ZnO NPs without capping; which revealed a reduction in the particle size and crystallinity in the structure of ZnO NPs [31]. Additionally, observed peaks around 10.39° and 20.61° in the XRD patterns of the CS-capped ZnO NPs, which was attributed to the crystal domain of CS, coincident with the pure compound (Fig. 1E) [32].

The morphology of ZnO NPs, commercialized and synthesized, with or without coating with CS, was evaluated by scanning electron microscopy (SEM). SEM images (Fig. 2) display that in all samples, ZnO NPs were agglomerated with uniform particle sizes. ZnO NPs were spherical with smooth surfaces, with an average size range of 15–90 nm for commercial ZnO NPs and 25–50 nm for synthesized ZnO NPs, respectively (Fig. 2A and B). On the other hand, SEM images of CS-capped ZnO NPs showed the polymeric surrounding shell onto the ZnO NPs surface, although the CS-capped commercially available ZnO NPs looks tight (Fig. 2C and D) in comparison with that one of the synthesized ZnO NPs. The tendency to increase particle size when incorporating CS was in agreement with the analysis previously carried out by DLS. However, some differences are observed in the values obtained by SEM since this technique does not allow determining the average diameter in the solvated state, therefore the observed sizes are smaller than those obtained by DLS [33].

The thermogravimetric analysis (TGA) allowed inferences about the structural organization of the organic coating onto the surface of ZnO NPs [34]. Fig. 3A and B displays the TGA and DTG plots of NPs, respectively, over a temperature range up to 600°C , under a nitrogen atmosphere. The commercial nanoparticles and the synthesized nanoparticles presented good thermal stability in the studied temperature range from 25 to 600°C (Fig. 3A and B (A and B)). An accumulative weight loss at 600°C of approximately 46 wt% was recorded for commercially available ZnO NPs coating with CS (Fig. 3A (C)). Meanwhile, the amount of the organic lost at 600°C for CS-capped synthesized ZnO NPs reached approximately 24 wt% (Fig. 3A (D)). Thus, in this last case, a more thermally stable coating was established on the surface of ZnO NPs. In both samples, the organic coating was left in multiple decomposition steps as can be seen in the DTG curves shown in Fig. 3B (C and D). Differences could be attributed to different conformations of the CS molecules around ZnO NPs, different binding sites, or the number of CS layers on the surface of ZnO NPs [22]. The thermal events of the raw materials CS (Fig. 3A and B (E)) and Zn acetate dihydrate (Fig. 3A and B (F)) coincide with what is described in the literature [35,36].

3.2. Antimicrobial evaluation

3.2.1. Minimum inhibitory concentration (MIC) and minimum bactericidal concentration (MBC) determinations

Commercial and synthesized ZnO NPs, with or without CS coating, were tested for their antibacterial activities against *S. aureus*, *E. coli*, *E. faecalis* and *P. aeruginosa* and results are shown in Table 2. MIC and MBC of GEN and zinc acetate dihydrate were also

Table 1

Average hydrodynamic particle size, polydispersity index (PDI), and zeta potential values (ζ -potential) obtained by DLS.

Sample	Size (nm) \pm SD	PDI \pm SD	ζ -potential (mV) \pm SD	Zn content (mg) /1 mg NPs \pm SD
Commercial ZnO NPs	108.0 \pm 28.0	0.22 \pm 0.08	-22.7 ± 1.2	0.73 \pm 0.01
Synthesized ZnO NPs	83.3 \pm 15.3	0.17 \pm 0.08	-22.5 ± 1.3	0.86 \pm 0.02
CS-coated commercially available ZnO NPs	135.0 \pm 15.0	0.24 \pm 0.07	33.2 \pm 3.8	0.26 \pm 0.01
CS-coated synthesized ZnO NPs	98.7 \pm 7.6	0.24 \pm 0.03	36.2 \pm 7.0	0.51 \pm 0.01

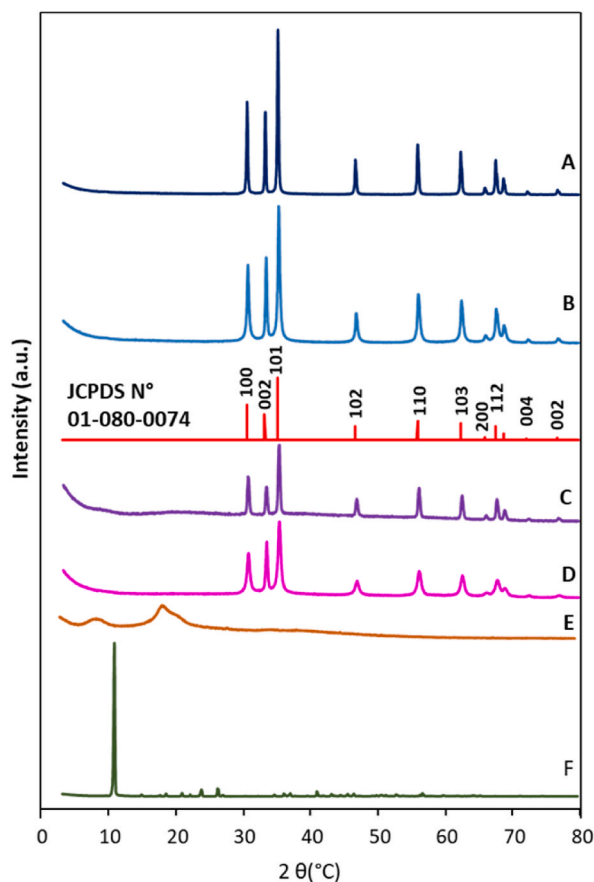


Fig. 1. X-ray diffraction (XRD) patterns of A. commercial ZnO NPs, B. synthesized ZnO NPs, C. CS-capped commercially available ZnO NPs, D. CS-capped synthesized ZnO NPs, E. CS, and F. zinc acetate dehydrate. The figure contains the diffractogram (red) of the JCPDS standard: 01-080-0074, hexagonal zinc oxide. (For interpretation of the references to color in this figure legend, the reader is referred to the Web version of this article.)

determined.

As shown in [Table 2](#), all NPs demonstrated increased antimicrobial activity against all bacterial strains tested in comparison to the precursor zinc acetate dihydrate used in the synthesis of the ZnO NPs. [Table 2](#) Despite that the MIC values of NPs ranged from 0.002 to 1.5 $\mu\text{g}/\text{mL}$, whereas the MIC range for the precursor salt was between 48.75 and 1560 $\mu\text{g}/\text{mL}$.

On the other hand, commercially available and synthesized ZnO NPs, with or without capping, showed different degrees of antibacterial activity among them concerning the bacterial species used herein, in some cases the MIC values obtained with the synthesized ZnO NPs slightly lower in comparison to commercially available ZnO NPs. Moreover, as shown in [Table 2](#), the CS-capped ZnO NPs showed even lower MIC values compared to those MIC values obtained with the uncapped ZnO NPs, being in some cases, the MIC values measured with the CS-capped synthesized ZnO NPs lower than the MIC values obtained with the CS-capped commercially available ZnO NPs.

On the other hand, it was tested the ability of NPs to kill the tested microorganisms; i.e., to demonstrate bactericidal activity by determining their MBC values. [Table 2](#) shows that the MBC results measured with all the samples evaluated against the 4 tested bacterial strains followed the same trend obtained with the MIC values measured. As shown in [Table 2](#), all NPs had an MBC/MIC ratio ≤ 4 , indicating that NPs were bactericidal.

In this work, it is also a remarkable fact that all ZnO NPs showed a very good antibacterial performance against both *P. aeruginosa* and *E. faecalis* in contrast to the results obtained in the report of Riahi et al. [37], who showed that the ZnO NPs they obtained did not show bacterial activity against these bacterial strains.

In summar, susceptibility data found in this work showed that the tested CS-capped synthesized ZnO NPs exhibited the highest antibacterial activity against the tested bacterial strains in comparison to CS-capped commercially available ZnO NPs, or the uncapped synthesized or commercially available ZnO NPs. These results allowed us to infer that the conformation of CS adsorbed on the ZnO NPs surface and probably, the smaller size of the synthesized ZnO NPs compared to the commercially available ones have a favorable effect on the antibacterial activity of these NPs.

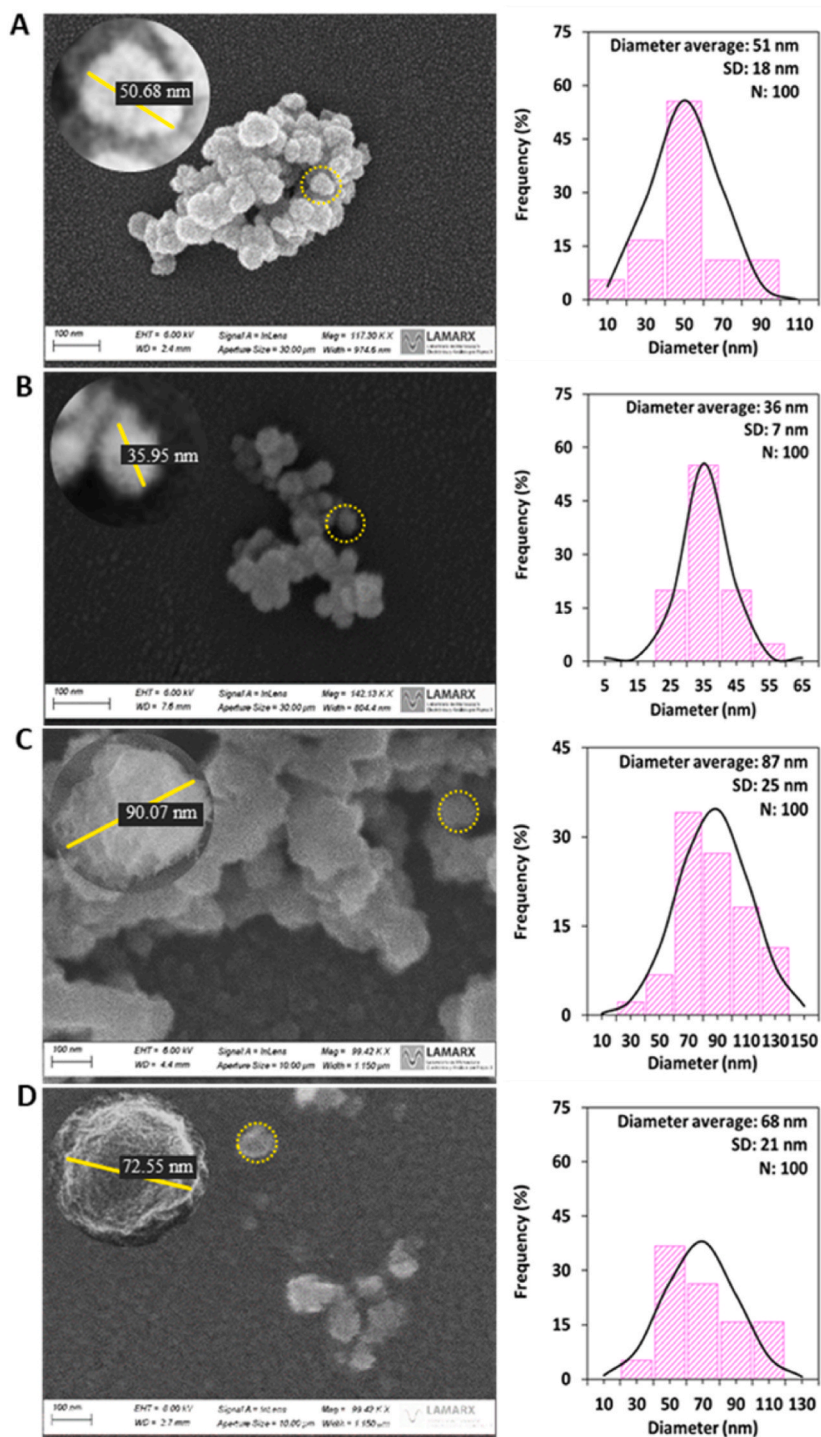


Fig. 2. Scanning electron microscopy (SEM) images and their respective size distribution histograms (diameter, nm) and Gaussian curve as a function of frequency (%) of A) commercial ZnO nanoparticles, B) synthesized ZnO nanoparticles, C) commercial ZnO NPs from CS-ZnO and D) synthesized nanoparticles from CS-ZnO. Scale: 100 nm. The inset circular images show an enlarged view of the nanoparticles with their respective diameter value acquired. The histograms were constructed by taking 100 nanoparticle diameter measurements with the ImageJ software. The respective averages and standard deviation are presented for each nanoparticle sample.

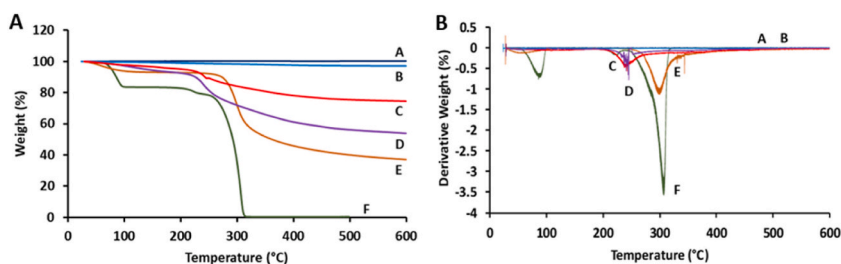


Fig. 3. Thermogravimetric plots recorded during thermal treatment up to 600 °C A) Weight (%) vs. temperature (°C) and B) Derivative weight (%) (DTG) for: A. ZnO NPs commercial, B. ZnO NPs synthesized, C. CS-capped synthesized ZnO NPs, D. CS-capped commercially available ZnO NPs, E. CS and F. zinc acetate dihydrate.

Table 2

Minimum inhibitory concentration (MIC) and minimum bactericidal concentration (MBC) values of different ZnO NPs formulations and Zn acetate salt, against *S. aureus*, *E. faecalis*, *P. aeruginosa*, and *E. coli* strains. Concentrations are expressed as the equivalent quantity of zinc ($\mu\text{g}/\text{mL}$).

	<i>S. aureus</i>			<i>E. faecalis</i>			<i>P. aeruginosa</i>			<i>E. coli</i>		
	MIC ($\mu\text{g}/\text{mL}$)	MBC ($\mu\text{g}/\text{mL}$)	MBC/MIC ratio	MIC ($\mu\text{g}/\text{mL}$)	MBC ($\mu\text{g}/\text{mL}$)	MBC/MIC ratio	MIC ($\mu\text{g}/\text{mL}$)	MBC ($\mu\text{g}/\text{mL}$)	MBC/MIC ratio	MIC ($\mu\text{g}/\text{mL}$)	MBC ($\mu\text{g}/\text{mL}$)	MBC/MIC ratio
<i>Zn acetate dihydrate</i>	48.75	48.75	1	1560	1560	1	97.5	97.5	1	97.5	97.5	1
Commercial ZnO NPs	0.4	0.8	2	0.08	0.08	1	1.5	1.5	1	0.01	0.01	1
Synthesized ZnO NPs	0.4	0.4	1	0.02	0.02	1	1.5	1.5	1	0.01	0.01	1
CS-coated commercially available ZnO NPs	0.08	0.08	1	0.0025	0.0025	1	0.08	0.08	1	0.04	0.04	1
CS-coated synthesized ZnO NPs	0.04	0.04	1	0.0025	0.0025	1	0.08	0.08	1	0.01	0.01	1
GEN	6.25	50	8	12.5	50	4	6.25	50	8	6.25	50	8

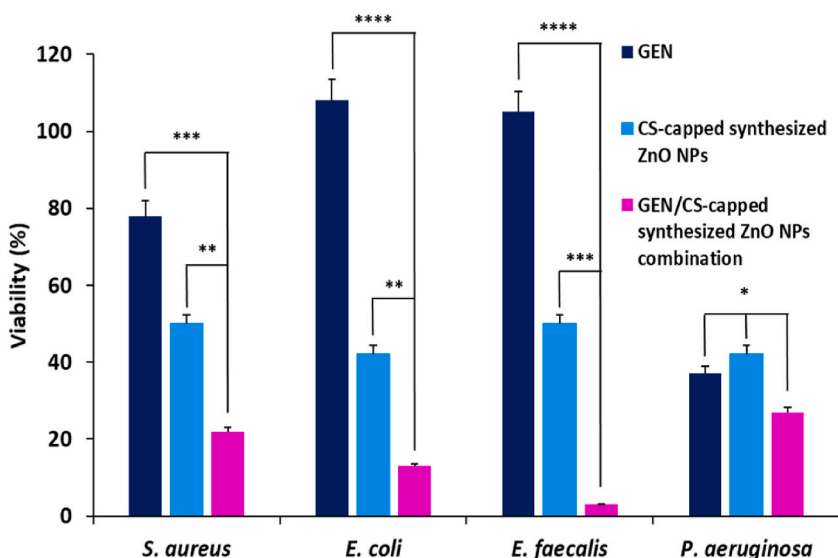


Fig. 4. Effect of GEN and CS-capped synthesized ZnO alone and their combination on the viability (%) of tested bacterial strains (mean \pm SD, $n = 3$, * $p < 0.05$, ** $p < 0.01$, *** $p < 0.001$, **** $p < 0.0001$). The concentrations ($\mu\text{g}/\text{mL}$) were defined by the synergistic activity, in *S. aureus* it was 0.012 and 0.02, *E. coli* 0.098 and 0.005, *E. faecalis* 0.78 and 0.001 and *P. aeruginosa* 0.049 and 0.005 for GEN and CS-ZnO synthesized NPs, respectively.

3.2.2. Checkerboard testing

The CS-capped ZnO NPs were selected to evaluate the interaction between NPs and GEN because these NPs showed better MIC and MBC values against the 4 tested bacterial strains compared to the rest of the NPs evaluated in this work. Fig. 4 shows the effects of GEN, and the combination of GEN with CS-capped synthesized ZnO NPs, on the susceptibility of tested bacterial strains. Although bacteria treated with GEN alone showed a decreasing percentage of bacterial viability, their survival was significantly reduced when combined with CS-capped synthesized ZnO NPs. For *S. aureus* the viability ranged from 78 to 22 %, for *E. coli* from 100 to 13 %, for *E. faecalis* from 100 to 2 %, and for *P. aeruginosa* from 37 to 27 % of GEN compared to the treatment in combination with NPs respectively.

Table 3 displays the checkerboard assay results used to assess the effects of CS-capped synthesized ZnO NPs on the antibiotic efficacy of GEN against *S. aureus*, *E. coli*, *E. faecalis*, and *P. aeruginosa*. As shown in Table 3, some combinations between CS-capped synthesized ZnO NPs and GEN inhibited the growth of all bacterial strains tested at much lower concentrations than GEN or NPs alone. For *S. aureus* GEN MIC value declined from 6.25 µg/mL to 0.012 µg/mL (1/525 MIC) and for CS-capped ZnO NPs, its MIC value was reduced from 0.04 µg/mL to 0.02 µg/mL (½ MIC). For *E. coli*, GEN MIC value decreased by 64 times, whereas for the NPs the decrease of its CIM value was 2-fold. In the case of *E. faecalis*, the MIC values decreased 16 and 2.5 times for GEN and NPs, respectively, and for *P. aeruginosa*, their MIC values decreased 128 and 32, respectively.

The results obtained in this study are in very close agreement with those obtained in the report of Hemmati et al. [28], who obtained a nanocomposite (CS–ZnO NPs) loaded with GEN and evaluated its antimicrobial and antibiofilm formation against *P. aeruginosa* and *S. aureus*. These authors showed a four-fold MIC reduction when these bacterial strains were treated with the GEN-loaded CS-ZnO nanocomposite in comparison with the MIC value of CS-ZnO nanocomposite alone. They found that for *P. aeruginosa*, the GEN nanocomposite MIC value decreased from 128 µg/mL to 0.5 µg/mL, while for *S. aureus*, the MIC value was reduced from 64 µg/mL to 0.125 µg/mL.

Comparing the results obtained in the present study of MIC values combining GEN with CS-capped ZnO NPs against *P. aeruginosa* and *S. aureus* with those MIC values obtained in the report of Hemmati et al. significantly lowest MIC values for the bacteria tested were found herein with the combined concentration levels of GEN and CS-capped ZnO NPs because of synergistic action of GEN and CS-capped ZnO NPs.

3.3. Determination of intracellular reactive oxygen species (ROS)

Table 4 and Fig. 5A–H summarize the measured levels of ROS after the preincubation of bacterial cells with GEN and CS-capped synthesized ZnO NPs alone, as well as in combination, respectively. There was an increase in ROS production after bacterial treatment with both GEN and NPs, compared to untreated (control) bacteria. Moreover, the increase in ROS levels was significantly higher when bacteria were treated with the combination of GEN and NPs, *S. aureus* (p-value 0.002), *E. coli* (p-value 0.003), and *E. faecalis* (p-value 0.004), with the difference being much greater with *P. aeruginosa* (p-value 0.0006). On the other hand, in the presence of ROS, green fluorescence is produced because of oxidation of the dye, which can be seen in Fig. 5A–D. Furthermore, enhanced ROS generation by the synergistic GEN/NPs combination was confirmed by intracellular ROS levels measurements in the presence of glutathione (GSH; a known ROS inhibitor). GSH can protect different cellular components by neutralizing ROS as it oxidizes into glutathione disulfide (GSSG) [38]. Fig. 5E–H and Table 4 display that the GEN/CS-capped synthesized ZnO NPs combination showed a notably higher GSH oxidation ability than GEN or CS-capped synthesized ZnO NPs alone, indicating that ROS generation by the combination was amplified concerning GEN or NPs themselves.

It is known that ROS can increase the sensitivity of bacteria to antimicrobial agents; e.i., Huang et al. [39], found that Fe⁺³ ions at low concentrations promoted the bactericidal effectiveness of GEN against *E. coli*. Results suggest that enhanced ROS production may

Table 3

Drug interactions between ZnO NPs synthesized capping with chitosan (CS) and gentamicin (GEN) against different bacterial strains in vitro.

Bacterial Strain	MIC _{GEN} (µg/mL)	MIC _{CS-capped synthesized ZnO NPs} (µg/mL)	C _{GEN} (µg/mL)	C _{CS-capped synthesized ZnO NPs} (µg/mL)	Change of MIC _{GEN}	Change of MIC _{CS-capped synthesized ZnO NPs}	FICI	Interaction
<i>S. aureus</i>	6.25	0.04	6.25	0.0025	NC	16	1.1	I
			6.25	0.005	NC	8	1.1	I
			6.25	0.01	NC	4	1.0	Ad
			0.012	0.02	521	2	0.3	S
<i>E. coli</i>	6.25	0.01	0.195	0.0025	32	4	0.3	S
			0.098	0.005	64	2	0.5	S
			0.78	0.001	16	2.5	0.5	S
<i>E. faecalis</i>	12.5	0.0025	0.049	0.0025	128	32	0.04	S
<i>P. aeruginosa</i>	6.25	0.08	0.049	0.005	128	16	0.07	S
			0.049	0.01	128	8	0.1	S
			0.049	0.02	128	4	0.3	S
			0.049	0.04	128	2	0.5	S

GEN: gentamicin, CS-capped synthesized ZnO NPs: zinc oxide nanoparticles synthesized capping with chitosan. FICI: fractional inhibitory concentration index. MIC: minimum inhibitory concentration.

MIC_{GEN} and MIC_{ZnO NPs}: MICs of GEN and ZnO NPs when used alone.

C_{GEN} and C_{ZnO NPs}: MICs of GEN and ZnO NPs when used in combination.

S: synergist, Ad: additive, I: indifferent.

Table 4

Intracellular levels of ROS (%) without GSH and with GSH of GEN, CS-capped synthesized ZnO NPs, and a combination of both in different bacterial strains: *S. aureus*, *E. coli*, *E. faecalis*, and *P. aeruginosa* with its respective reduction in ROS production (%)

Bacterial Strain	Sample	ROS \pm SD (%) without GSH	ROS \pm SD (%) with GSH	Reduction in ROS production by GSH (%)
<i>S. aureus</i>	GEN	20 \pm 4	4 \pm 4	81 \pm 3
	CS-capped synthesized ZnO NPs	22 \pm 3	1 \pm 1	96 \pm 4
	GEN + CS-capped synthesized ZnO NPs	30 \pm 1	1 \pm 1	97 \pm 5
<i>E. coli</i>	GEN	7 \pm 6	3 \pm 5	61 \pm 5
	CS-capped synthesized ZnO NPs	17 \pm 2	0 \pm 3	100 \pm 1
	GEN + CS-capped synthesized ZnO NPs	18 \pm 1	1 \pm 5	95 \pm 4
<i>E. faecalis</i>	GEN	9 \pm 1	3 \pm 4	69 \pm 2
	CS-capped synthesized ZnO NPs	10 \pm 2	1 \pm 4	91 \pm 3
	GEN + CS-capped synthesized ZnO NPs	18 \pm 2	1 \pm 5	93 \pm 4
<i>P. aeruginosa</i>	GEN	15 \pm 3	3 \pm 1	77 \pm 5
	CS-capped synthesized ZnO NPs	12 \pm 4	0.3 \pm 2.3	97 \pm 3
	GEN + CS-capped synthesized ZnO NPs	25 \pm 2	2 \pm 2	92 \pm 2

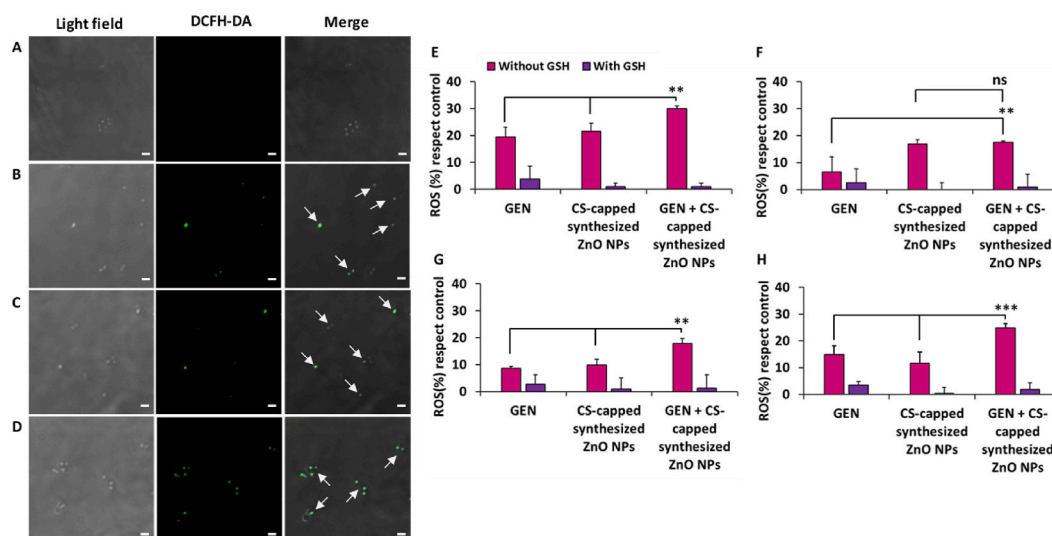


Fig. 5. Photographs obtained by fluorescence microscopy representative of the production of intracellular ROS in the *S. aureus* bacterial strain. The DCFH-DA marker (green) is an indicator of greater ROS production. A. Control, B. GEN, C. CS-capped synthesized ZnO NPs and D. CS-capped synthesized ZnO NPs combined with GEN. Scale bar: 1 μ m. The white arrows indicate bacteria with ROS production. On the other hand, bar graphs represent intracellular levels of ROS (%) without GSH (pink) and with GSH (purple) of GEN, CS-capped synthesized ZnO NPs, and a combination of both in different bacterial strains: E. *S. aureus*, F. *E. coli*, G. *E. faecalis* and H. *P. aeruginosa* (mean \pm SD, n = 3, ns: no significant difference, **p < 0.01, ***p < 0.001). (For interpretation of the references to color in this figure legend, the reader is referred to the Web version of this article.)

be partly responsible for the synergistic effects of the combined CS-capped ZnO NPs/GEN.

3.4. Intracellular uptake of ZnO NPs by bacterial cells

Fig. 6A–D shows the zinc accumulation in bacterial cells treated with commercially available and synthesized ZnO NPs, CS-capped of both kinds of ZnO NPs, and zinc acetate dihydrate after 1 h of incubation at 37 $^{\circ}$ C.

Higher intracellular zinc accumulation was observed when bacterial cells were treated with CS-capped ZnO NPs in comparison to uncapped ZnO NPs or the zinc salt, which might be because of CS coating produced a highly positive surface charge onto the ZnO NPs compared to the uncapped ZnO NPs, which had a negative surface charge (Table 1). CS-capped ZnO NPs might be electrostatically attracted to the anionic cell wall of bacterial cells more effectively than the uncapped ZnO NPs, even more than Zn^{2+} ions. Additionally, the positive surface charge of CS-capped synthesized ZnO NPs was even higher than that of CS-capped commercially available ZnO NPs (Table 1). Therefore, the difference in particle charge surface could have contributed to the higher zinc accumulation inside

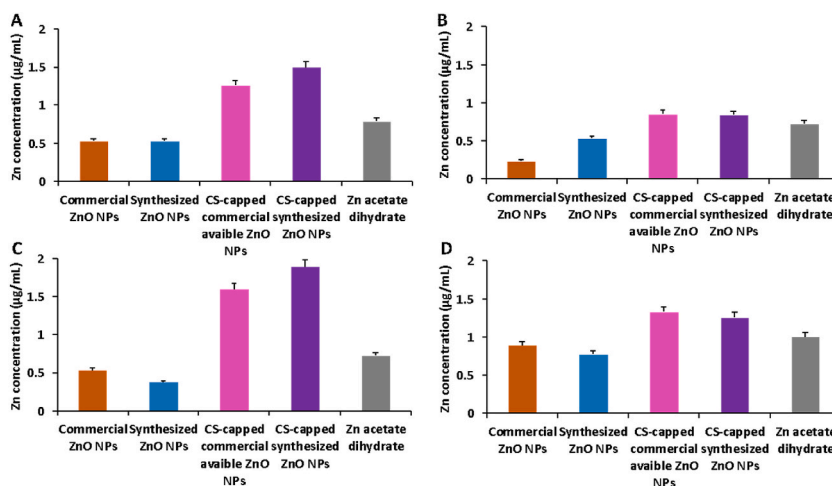


Fig. 6. Intracellular uptake of the different ZnO NPs formulations in tested bacterial strains: *A. S. aureus*, *B. E. coli*, *C. E. faecalis*, and *D. P. aeruginosa* (mean \pm SD, $n = 3$).

the bacterial cells and the overproduction of ROS by bacteria.

On the other hand, differences in the zinc accumulation between Gram-positive (Fig. 6A and C) and Gram-negative bacteria (Fig. 6B and D) were also shown. Although the zeta-potential value of both Gram-positive and Gram-negative bacteria is negative, differences might be attributed to the structural disparity in cell wall composition between these kinds of bacteria [40–42]. Results were also in agreement with the higher ROS production obtained with the Gram-positive bacteria in comparison to the Gram-negative bacteria tested herein.

3.5. Intracellular uptake of GEN combined with synthesized CS-capped ZnO NPs by bacterial cells

3.5.1. Validation of an indirect UV–visible spectrophotometric method for gentamicin quantification

Table 5 presents the outcomes derived from various validation parameters for the indirect colorimetric method employed in the quantification of Gentamicin (GEN). The interaction of Ninhydrin (NIN) with the amino acids of GEN results in the formation of a purple complex (GEN-NIN). Initially, the specificity or selectivity of the method was established. UV spectra for all components were acquired separately (NIN alone, GEN alone, bacterial supernatants with and without NIN, ZnO NPs synthesized with CS capping (with and without NIN)), revealing no interferences. The wavelength of maximum absorption for the complex was identified as 400 nm. With bacterial supernatants, a peak at approximately λ 260 nm, attributed to RNA and DNA nucleic bases, was observed. Synthesized ZnO NPs covered with CS exhibited an absorption maximum of around λ 360 nm. However, because of their breakdown during the quantification process, the final sample contained Zn rather than ZnO. As free Zn does not absorb in the UV–visible range, no interference was observed, allowing for the determination of the GEN-NIN complex at λ 400 nm.

The calibration curve is fitted linearly by the least squares method with an r^2 of 0.9996. Sensitivity was gauged through the calculation of the LOD) and LOQ, yielding values of $0.0432 \pm 0.0001 \mu\text{g/mL}$ and $3.125 \pm 0.005 \mu\text{g/mL}$, respectively. Accuracy fell within the range of 97%–101% across the three tested concentrations. Precision, assessed as both intra-day and inter-day precision at three quality control levels, was less than 2%. These findings affirm that the method adheres to the requisite validation standards for GEN quantification.

3.5.2. Quantification of intracellular gentamicin

As observed in Fig. 7 there was an increase in GEN uptake into bacterial cells when combined with the CS-capped synthesized ZnO NPs in comparison to GEN alone. Moreover, the difference was even larger with the Gram-negative bacteria *E. coli* compared with the other bacteria strains tested. These results might be ascribed to membrane damage of the bacteria cells produced by the CS-capped synthesized ZnO NPs, since it is known that ZnO NPs can disrupt the bacterial cell membrane thus allowing a greater internalization of the antibiotic by the bacterial cells [37].

GEN exerts its antibacterial action through an irreversible binding with mRNA and therefore inhibiting the synthesis of proteins in bacteria [43]. Hence, the enhanced amount of GEN getting access to bacterial cytosol will determine that bacteria is more susceptible to this antibiotic [44].

4. Conclusions

The current investigation reveals that the combination of ZnO NPs with GEN yields robust synergistic bactericidal effects. Notably, the ZnO NPs with chitosan (CS) coating emerge as the most efficacious in eliciting this phenomenon. This heightened efficacy is

Table 5

Method validation parameters (mean \pm SD; n = 3) Levels of gentamicin concentration ($\mu\text{g/mL}$) low: L: 3.125, medium: M: 25, high: H: 100. r^2 : linear coefficient correlation.

Parameter	Concentration	Result
Selectivity		
Maximum absorption wavelength (nm)		400
		No interference observed
Linearity		
Regression equation ($\mu\text{g/mL}$)		$y = 0.0015x - 0.0432$
r^2		0.9996
Sensibility		
LOD $\mu\text{g/mL}$		0.0432 ± 0.0001
LOQ $\mu\text{g/mL}$		3.125 ± 0.005
Accuracy (% recovery)		
	L	97 ± 6
	M	99 ± 4
	H	101 ± 3
Precision (% RSD)		
<i>Intra-day</i>		
	L	0.5922 ± 0.0003
	M	1.908 ± 0.002
	H	1.728 ± 0.003
<i>Inter-day</i>		
	L	0.4221 ± 0.0002
	M	1.679 ± 0.001
	H	1.324 ± 0.003

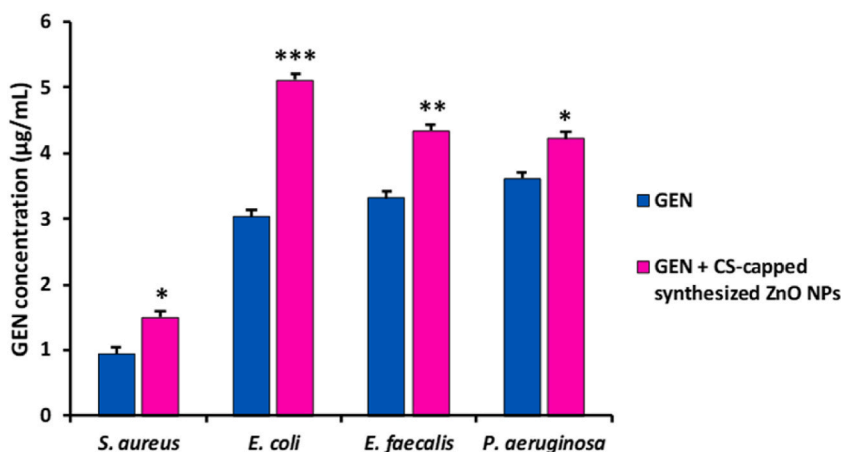


Fig. 7. Intracellular uptake of GEN alone and combined with CS-capped synthesized ZnO NPs in tested bacterial strains (mean \pm SD, n = 3, *p < 0.05, **p < 0.01, ***p < 0.001).

attributed to the conformational coating of CS onto the surface of the NPs, which imparts the highest positive surface charge. This characteristic likely facilitates enhanced proximity between ZnO NPs and microorganisms, surpassing the effectiveness of other NPs examined in this study. Consequently, this interaction leads to heightened internalization of zinc and GEN into bacterial cells, accompanied by an intracellular overproduction of reactive oxygen species (ROS).

In conclusion, the bactericidal synergistic combination between GEN and CS-capped synthesized ZnO NPs might be a powerful therapeutic alternative for repositioning the first-line antibiotic GEN.

Future research will explore combinations of GEN with NPs for resistant bacterial strains. Furthermore, it would be important to determine the cytotoxicity in eukaryotic cells of these combinations.

Author contributions

Paulina Páez: Writing – review & editing, Supervision, Methodology, Data curation. Gladys Granero: Writing – review & editing, Writing – original draft, Supervision, Project administration, Funding acquisition, Formal analysis, Conceptualization. Ivana Scolari: Writing – review & editing, Methodology, Investigation

Data availability statement

Data associated with the study have not been deposited into a publicly available repository because they have been included in the article.

Declaration of competing interest

The authors declare that they have no known competing financial interests or personal relationships that could have appeared to influence the work reported in this paper.

Acknowledgments

Authors acknowledge Consejo Nacional de Investigaciones Científicas y Técnicas (CONICET), Argentina, Secretaría de Ciencia y Técnica - Universidad Nacional de Córdoba, Argentina (SECyT-UNC) and Fondo para la Investigación Científica y Tecnológica (FONCYT), Argentina, for providing the support and the facilities for this study.

References

- [1] S. Luo, X. Kang, X. Luo, C. Li, G. Wang, Study on the inhibitory effect of quercetin combined with gentamicin on the formation of *Pseudomonas aeruginosa* and its bioenvelope, *Microb. Pathog.* 182 (2023), <https://doi.org/10.1016/j.micpath.2023.106274>.
- [2] Antimicrobial Resistance Collaborators, Global burden of bacterial antimicrobial resistance in 2019: a systematic analysis, *Lancet* 400 (2022) 1102, [https://doi.org/10.1016/S0140-6736\(21\)02653-2](https://doi.org/10.1016/S0140-6736(21)02653-2).
- [3] M. Jiang, X. Li, C.L. Xie, P. Chen, W. Luo, C. Xiao Lin, Q. Wang, D.M. Shu, C. Long Luo, H. Qu, J. Ji, Fructose-enabled killing of antibiotic-resistant *Salmonella enteritidis* by gentamicin: insight from reprogramming metabolomics, *Int. J. Antimicrob. Agents* 62 (2023), <https://doi.org/10.1016/j.ijantimicag.2023.106907>.
- [4] Y. Zhou, Y. Yong, C. Zhu, H. Yang, B. Fang, Exogenous D-ribose promotes gentamicin treatment of several drug-resistant *Salmonella*, *Front. Microbiol.* 13 (2022), <https://doi.org/10.3389/fmicb.2022.1053330>.
- [5] S.N. Leonard, M.E. Supple, R.G. Gandhi, M.D. Patel, Comparative activities of telavancin combined with nafcillin, imipenem, and gentamicin against *Staphylococcus aureus*, *Antimicrob. Agents Chemother.* 57 (2013) 2678–2683, <https://doi.org/10.1128/AAC.02127-12>.
- [6] A.I. Ribeiro, A.M. Dias, A. Zille, Synergistic effects between metal nanoparticles and commercial antimicrobial agents: a review, *ACS Appl. Nano Mater.* 5 (2022) 3030–3064, <https://doi.org/10.1021/acsnano.1c03891>.
- [7] K.S. Siddiqi, A. ur Rahman, Tajuddin, A. Husen, Properties of zinc oxide nanoparticles and their activity against microbes, *Nanoscale Res. Lett.* 13 (2018), <https://doi.org/10.1186/s11671-018-2532-3>.
- [8] M. Izzi, M.C. Sportelli, L. Torsi, R.A. Picca, N. Cioffi, Synthesis and antimicrobial applications of ZnO nanostructures: a review, *ACS Appl. Nano Mater.* 6 (2023) 10881–10902, <https://doi.org/10.1021/acsnano.3c01432>.
- [9] D. Visinescu, M.D. Hussien, J.C. Moreno, R. Negrea, R. Birjega, S. Somacescu, C.D. Ene, M.C. Chifiriuc, M. Popa, M.S. Stan, O. Carp, Zinc oxide spherical-shaped nanostructures: investigation of surface reactivity and interactions with microbial and mammalian cells, *Langmuir* 34 (2018) 13638–13651, <https://doi.org/10.1021/acs.langmuir.8b02528>.
- [10] Food and Drug Administration (FDA), Department of health and human services, code of federal regulations - title 21 - Food and drugs, PART 182 – SUBSTANCES GENERALLY RECOGNIZED AS SAFE. <https://www.accessdata.fda.gov/scripts/cdrh/cfdocs/cfcfr/cfsearch.cfm?fr=182.8991>, 2023. (Accessed 1 October 2023).
- [11] N. Mistry, R. Bandyopadhyaya, S. Mehra, ZnO nanoparticles and rifampicin synergistically damage the membrane of mycobacteria, *ACS Appl. Nano Mater.* 3 (2020) 3174–3184, <https://doi.org/10.1021/acsnano.9b02089>.
- [12] R.S. Kurup, E. Cherian, P.C. Thomas, Synthesis of ZnO nanoparticle and evaluation of its potential to enhance the activity of antibiotics, *IOP Conf. Ser. Mater. Sci. Eng.* 360 (2018) 012001, <https://doi.org/10.1088/1757-899X/360/1/012001>.
- [13] M.A.A. Agreles, I.D.L. Cavalcanti, I.M.F. Cavalcanti, Synergism between metallic nanoparticles and antibiotics, *Appl. Microbiol. Biotechnol.* 106 (2022) 3973–3984, <https://doi.org/10.1007/s00253-022-12001-1>.
- [14] Y. Wang, J. Xu, C. Yu, X. Zhou, L. Chang, J. Liu, Q. Peng, Prevention of bacterial biofilm formation on orthodontic brackets by non-crosslinked chitosan coating, *Int. J. Biol. Macromol.* 251 (2023) 126283, <https://doi.org/10.1016/j.ijbiomac.2023.126283>.
- [15] Y. Lin, J. Xu, Y. Dong, Y. Wang, C. Yu, Y. Li, C. Zhang, Q. Chen, S. Chen, Q. Peng, Drug-free and non-crosslinked chitosan/hyaluronic acid hybrid hydrogel for synergistic healing of infected diabetic wounds, *Carbohydr. Polym.* 314 (2023) 120962, <https://doi.org/10.1016/j.carbpol.2023.120962>.
- [16] X. Tang, J. Liu, R. Yan, Q. Peng, Carbohydrate polymer-based bioadhesive formulations and their potentials for the treatment of ocular diseases: a review, *Int. J. Biol. Macromol.* 242 (2023) 124902, <https://doi.org/10.1016/j.ijbiomac.2023.124902>.
- [17] T. Wu, Q. Zhou, G. Hong, Z. Bai, J. Bian, H. Xie, C. Chen, A chlorogenic acid-chitosan complex bifunctional coating for improving osteogenesis differentiation and bactericidal properties of zirconia implants, *Colloids Surf. B Biointerfaces* 230 (2023) 113484, <https://doi.org/10.1016/j.colsurfb.2023.113484>.
- [18] Y. Dong, J. Liu, Y. Chen, T. Zhu, Y. Li, C. Zhang, X. Zeng, Q. Peng, Photothermal and natural activity-based synergistic antibacterial effects of Ti3C2Tx MXene-loaded chitosan hydrogel against methicillin-resistant *Staphylococcus aureus*, *Int. J. Biol. Macromol.* 240 (2023) 124482, <https://doi.org/10.1016/j.ijbiomac.2023.124482>.
- [19] I.R. Scolari, P.L. Páez, M.M. Musri, J.P. Petiti, A. Torres, G.E. Granero, Rifampicin loaded in alginate/chitosan nanoparticles as a promising pulmonary carrier against *Staphylococcus aureus*, *Drug Deliv Transl Res* 10 (2020) 1403–1417, <https://doi.org/10.1007/s13346-019-00705-3>.
- [20] S.M. Andrabi, A. Kumar, A kaolin/calcium incorporated shape memory and antimicrobial chitosan-dextran based cryogel as an efficient haemostatic dressing for uncontrolled hemorrhagic wounds, *Biomater. Adv.* 150 (2023) 213424, <https://doi.org/10.1016/j.bioadv.2023.213424>.
- [21] CLSI, *Performance Standards for Antimicrobial Susceptibility Testing*, CLSI Supplement M100, 30th ed., Clinical and Laboratory Standards Institute., Wayne, PA, 2020, 30th ed.,
- [22] I. Eleftheriadou, K. Giannousi, E. Protonotariou, L. Skoura, M. Arsenakis, C. Dendrinou-Samara, A. Sivropoulou, Cocktail of CuO, ZnO, or CuZn nanoparticles and antibiotics for combating multidrug-resistant *Pseudomonas aeruginosa* via efflux pump inhibition, *ACS Appl. Nano Mater.* 4 (2021) 9799–9810, <https://doi.org/10.1021/acsnano.1c02208>.
- [23] F.U. Khan, Y. Chen, N.U. Khan, A. Ahmad, K. Tahir, Z.U. Khan, A.U. Khan, S.U. Khan, M. Raza, P. Wan, Visible light inactivation of *E. coli*, Cytotoxicity and ROS determination of biochemically capped gold nanoparticles, *Microb. Pathog.* 107 (2017) 419–424, <https://doi.org/10.1016/j.micpath.2017.04.024>.
- [24] P.L. Páez, M.C. Becerra, I. Albesa, Effect of the association of reduced glutathione and ciprofloxacin on the antimicrobial activity in *Staphylococcus aureus*, *FEMS Microbiol. Lett.* 303 (2010) 101–105, <https://doi.org/10.1111/j.1574-6968.2009.01867.x>.
- [25] International Council for Harmonisation of Technical Requirements for Pharmaceuticals for Human Use, *VALIDATION OF ANALYTICAL PROCEDURES Q2(R2)*, 2022.

- [26] Food and Drug Administration (Fda), M10 BIOANALYTICAL METHOD VALIDATION and STUDY SAMPLE ANALYSIS Guidance for Industry, 2022. <https://www.fda.gov/vaccines-blood-biologics/guidance-compliance-regulatory-information-biologics/biologics-guidances>.
- [27] P. Frutos, S. Torrado, M.E. Perez-Lorenzo, G. Frutos, A Validated Quantitative Colorimetric Assay for Gentamicin, 2000. www.elsevier.com/locate/jpba.
- [28] F. Hemmati, R. Salehi, R. Ghotaslou, H.S. Kafil, A. Hasani, P. Gholizadeh, M.A. Rezaee, The assessment of antibiofilm activity of chitosan-zinc oxide-gentamicin nanocomposite on *Pseudomonas aeruginosa* and *Staphylococcus aureus*, *Int. J. Biol. Macromol.* 163 (2020) 2248–2258, <https://doi.org/10.1016/j.ijbiomac.2020.09.037>.
- [29] A. Zare, A. Saadati, S. Shebani, Modification of a Z-scheme ZnO-CuO nanocomposite by Ag loading as a highly efficient visible light photocatalyst, *Mater. Res. Bull.* 158 (2023) 112048, <https://doi.org/10.1016/j.materresbull.2022.112048>.
- [30] P. Bindu, S. Thomas, Estimation of lattice strain in ZnO nanoparticles: X-ray peak profile analysis, *Journal of Theoretical and Applied Physics* 8 (2014) 123–134, <https://doi.org/10.1007/s40094-014-0141-9>.
- [31] Mohd Shkir, B.M. Al-Shehri, M.P. Pachamuthu, A. Khan, K.V. Chandekar, S. AlFaify, M.S. Hamdy, A remarkable improvement in photocatalytic activity of ZnO nanoparticles through Sr doping synthesized by one pot flash combustion technique for water treatments, *Colloids Surf. A Physicochem. Eng. Asp.* 587 (2020) 124340, <https://doi.org/10.1016/j.colsurfa.2019.124340>.
- [32] R. Varma, S. Vasudevan, Extraction, characterization, and antimicrobial activity of chitosan from horse mussel *Modiolus modiolus*, *ACS Omega* 5 (2020) 20224–20230, <https://doi.org/10.1021/acsomega.0c01903>.
- [33] E.V. Kuznetsova, N.M. Kuznetsov, K.T. Kalinin, P.V. Lebedev-Stepanov, A.A. Novikov, S.N. Chvalun, The role of integrated approach in the determination of nanoparticle sizes in dispersions, *Colloid J.* 84 (2022) 704–714, <https://doi.org/10.1134/S1061933X22600348>.
- [34] K. Giannousi, E. Hatzivassiliou, S. Mourdikoudis, G. Vourlias, A. Pantazaki, C. Dendrinou-Samara, Synthesis and biological evaluation of PEGylated CuO nanoparticles, *J. Inorg. Biochem.* 164 (2016) 82–90, <https://doi.org/10.1016/j.jinorgbio.2016.09.003>.
- [35] H. Moussout, M. Aazza, H. Ahlafi, Thermal degradation characteristics of chitin, chitosan, Al₂O₃/chitosan, and benonite/chitosan nanocomposites, in: *Handbook of Chitin and Chitosan*, Elsevier, 2020, pp. 139–174, <https://doi.org/10.1016/B978-0-12-817968-0.00005-6>.
- [36] N. Horzum, M.E. Hilal, T. Isik, Enhanced bactericidal and photocatalytic activities of ZnO nanostructures by changing the cooling route, *New J. Chem.* 42 (2018) 11831–11838, <https://doi.org/10.1039/c8nj01849a>.
- [37] S. Riahi, N. Ben Moussa, M. Lajnef, N. Jebari, A. Dabek, R. Chtourou, G. Guisbiers, S. Vimont, E. Herth, Bactericidal activity of ZnO nanoparticles against multidrug-resistant bacteria, *J. Mol. Liq.* 387 (2023) 122596, <https://doi.org/10.1016/j.molliq.2023.122596>.
- [38] C. Hwang, M.-H. Choi, H.-E. Kim, S.-H. Jeong, J.-U. Park, Reactive oxygen species-generating hydrogel platform for enhanced antibacterial therapy, *NPG Asia Mater.* 14 (2022) 72, <https://doi.org/10.1038/s41427-022-00420-5>.
- [39] Y. feng Huang, Y. Li, J. ying Chen, J. hui Lin, L. Liu, J. zhou Ye, Y. bin Su, Promoting effect of Fe³⁺ on gentamicin resistance in *Escherichia coli*, *Biochem. Biophys. Res. Commun.* 625 (2022) 134–139, <https://doi.org/10.1016/j.bbrc.2022.07.102>.
- [40] T.J. Silhavy, D. Kahne, S. Walker, The bacterial cell envelope, *Cold Spring Harbor Perspect. Biol.* 2 (2010), <https://doi.org/10.1101/cshperspect.a000414> a000414–a000414.
- [41] M. Jin, B. He, X. Cai, Z. Lei, T. Sun, Research progress of nanoparticle targeting delivery systems in bacterial infections, *Colloids Surf. B Biointerfaces* 229 (2023) 113444, <https://doi.org/10.1016/j.colsurfb.2023.113444>.
- [42] Y. Xu, H. Li, X. Li, W. Liu, What happens when nanoparticles encounter bacterial antibiotic resistance? *Sci. Total Environ.* 876 (2023) 162856 <https://doi.org/10.1016/j.scitotenv.2023.162856>.
- [43] P. Varvarà, C. Calà, C.M. Maida, M. Giuffrè, N. Mauro, G. Cavallaro, Arginine-rich peptidomimetic ampicillin/gentamicin conjugate to tackle nosocomial biofilms: a promising strategy to repurpose first-line antibiotics, *ACS Infect. Dis.* 9 (2023) 916–927, <https://doi.org/10.1021/acsinfectdis.2c00579>.
- [44] S. Chakraborti, A.K. Mandal, S. Sarwar, P. Singh, R. Chakraborty, P. Chakrabarti, Bactericidal effect of polyethyleneimine capped ZnO nanoparticles on multiple antibiotic resistant bacteria harboring genes of high-pathogenicity island, *Colloids Surf. B Biointerfaces* 121 (2014) 44–53, <https://doi.org/10.1016/j.colsurfb.2014.03.044>.